CONFORMAL GRATING ELECTROMECHANICAL SYSTEM (GEMS) FOR HIGH-SPEED DIGITAL LIGHT MODULATION

Marek W. Kowarz, John C. Brazas, Jr., and James G. Phalen

Integrated Materials and Microstructures Laboratory, Eastman Kodak Company
1999 Lake Ave., Rochester, NY 14650-2015, USA
Phone: (585) 588-4160, Fax: (585) 722-9053, E-mail: marek.kowarz@kodak.com

ABSTRACT

A diffractive optical MEMS device for spatial and temporal light modulation is described that is capable of high-speed digital operation. The device contains electromechanical ribbons suspended flat above a silicon substrate by a periodic series of intermediate supports. When actuated electrostatically, the ribbons conform around the support substructure to produce a grating. The device has optical switching times of less than 50 nsec, sub-nanosecond jitter, high optical contrast and efficiency, and reliable actuation in contact mode. The fine gray levels needed for digital imaging systems are produced by pulse width modulation.

INTRODUCTION

Electromechanical gratings are important for a wide range of applications, including display, data storage, spectroscopy, and printing. These systems require large numbers of individually addressable pixels in either a linear or area array. Over one million pixels are desirable for a high-quality display system with an area spatial light modulator. Two distinctively different types of spatial light modulators containing arrays of electromechanical grating pixels are well known and were under development over a number of years: viscoelastic membrane devices [1,2] and the grating light valves (GLV) of Silicon Light Machines [3,4]. Both of these modulator technologies use electrostatic actuation to produce surface deformations. Viscoelastic membrane devices utilize a metallized elastomer gel that is deformed to produce a sinusoidal grating profile, whereas GLVs have interdigitated suspended ribbons of metallized silicon nitride that are selectively deformed to produce a square grating profile.

This paper describes the design, theory of operation, and performance of a conformal grating electromechanical system (GEMS). The conformal GEMS device is a new design for a spatial light modulator based on diffractive optical MEMS technology. The device provides high-speed digital light modulation with high contrast and good throughput.

DEVICE DESIGN AND OPERATION

The design and operation of a conformal GEMS device [5] fabricated on a silicon substrate are shown in Figs. 1 and 2. The structural design consists of tensile electromechanical ribbons suspended over a number of identical parallel channels. The channels are separated by intermediate supports, which have a periodic spacing Λ. This periodic substructure is completely hidden under the ribbons. A single pixel in a linear array typically has one or more suspended ribbons, each attached to several intermediate supports. There is no fundamental limit on the number of ribbons or intermediate supports per pixel. Figure 2a could, therefore, represent a single pixel of four ribbons or four adjacent pixels, if the ribbon metal were appropriately patterned for electrical addressability.

In the unactuated state, with no voltage difference between the ribbon metal and the substrate, the ribbons are suspended flat in tension and the device functions as a plane mirror (see Fig. 1). To actuate the device, a voltage is applied between the ribbon metal and the silicon substrate, causing the ribbons to deform electrostatically into the parallel channels to reveal the substructure hidden below, as depicted in Figs. 2a and 2b. When the device is fully actuated, the ribbons contact standoffs on the substrate that reduce the potential area of contact and, thus, the likelihood of ribbon failure by stiction. The semiconformal grating formed by this ribbon deformation has a trapezoidal-like profile with a period Λ. The grating profile in Fig. 2b is calculated using an electromechanical model, assuming high tensile stress. Figures 1c and 2c are interferometric measurements showing ribbon surface topography of the unactuated and fully actuated states.

The device described here is designed to function as a digital spatial light modulator by switching between the unactuated and fully actuated states. In the actuated state, an incident light beam is diffracted into multiple orders as illustrated in Fig. 2a. Most of the optical energy appears in the four orders shown (-2nd, -1st, 1st, and 2nd). Depending on the design of the optical system that utilizes the device, one or more of these diffracted orders can be captured. For applications that require high contrast and good throughput, the reflected beam
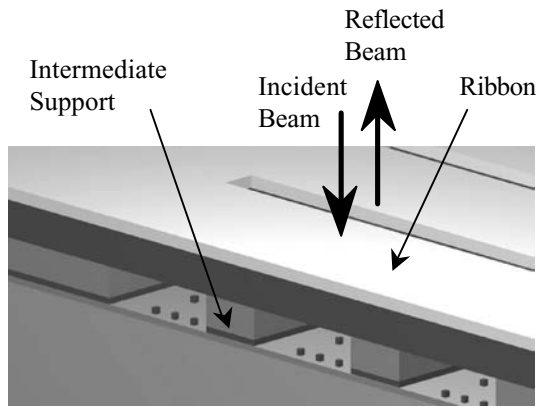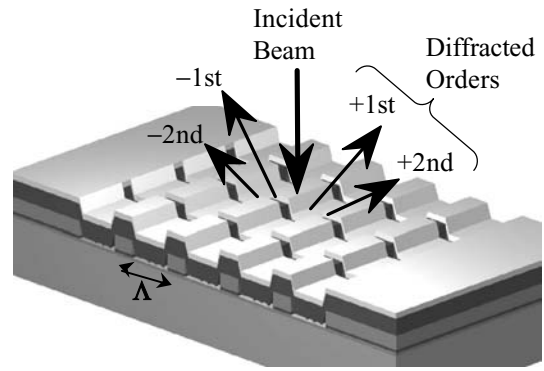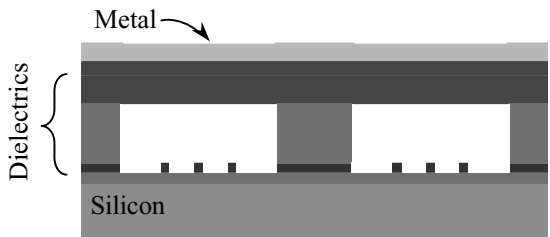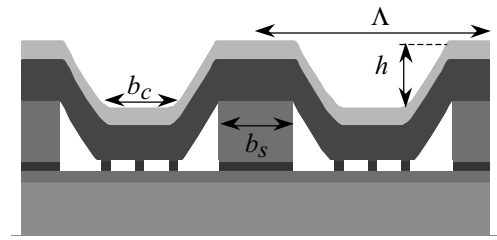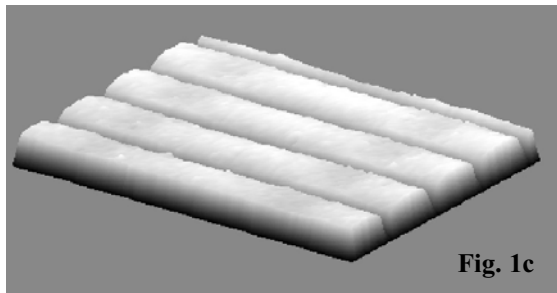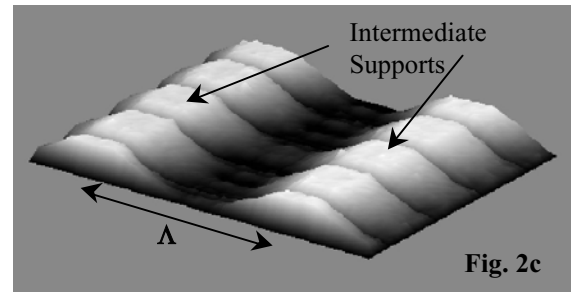
Fig. 1a

Fig. 1b

Fig. 1c

Fig. 1 Illustration of a conformal GEMS device in the unactuated state (Figs. 1a and 1b) with interferometry showing ribbon topography of a fabricated device (Fig. 1c, courtesy of Rob Gutierrez). For clarity, the vertical scale is greatly amplified relative to the horizontal.

(0th order) is blocked and all other diffracted orders are collected. Contrast is increased by minimizing the protrusion of the intermediate supports above the surface of the device.

In our typical devices, the ribbons are formed from high stress silicon nitride with a highly reflecting thin metal surface. The remaining layers are dielectrics selected to have good etch-selectivity differences to allow patterning of the key features. For visible wavelengths, typical periods are between 15 and 50 μm, air gaps are between 150 and 200 nm, ribbon widths are up to 20 μm.

Fig. 2a

Fig. 2b

Fig. 2c

Fig. 2 Illustration of a conformal GEMS device in the actuated state (Figs. 2a and 2b) with interferometry showing the semi-conformal ribbon topography of the grating formed by a fabricated device (Figs. 2c).

Figure 3a is a photograph of a packaged conformal GEMS linear array with 256 pixels that is a fully functional prototype. To form the linear array, the grating period Λ of each pixel is oriented perpendicular to the array direction as shown in Figs. 3b and 3c. In comparison to the GLV array [4], this perpendicular orientation provides more flexibility in collecting diffracted orders and increases alignment tolerances. In addition, the cost of the optical system is less because smaller optical components can be used. Figure 3b shows a 20-pixel portion of the array with the state of each pixel indicated by a 1 or 0 to denote the fully actuated or unactuated state, respectively. Visible in the magnified view in Fig. 3c, each pixel contains 8 ribbons
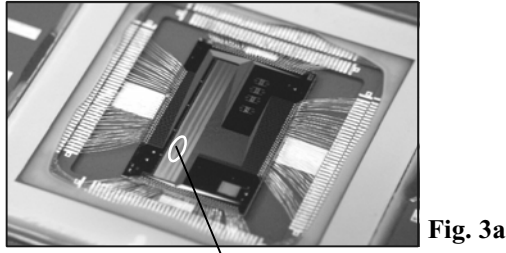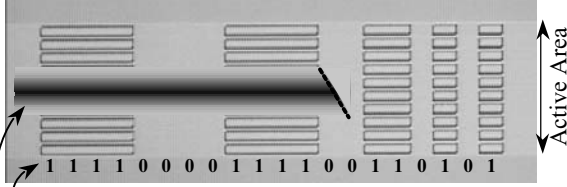
Fig. 3a

Enlarged Area
of 20 Pixels

Fig. 3b

Active Area

1 1 1 1 0 0 0 0 1 1 1 1 0 0 1 1 0 1 0 1

Pixel
Sequence

Laser
Illumination
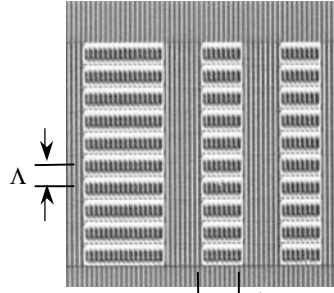
Enlarged to Show
Individual Ribbons

Λ

Fig. 3c

1 Pixel

Fig. 3 Photograph of a packaged prototype linear array (Fig. 3a) and two interference micrographs (Figs. 3b and 3c) showing an actuated pixel sequence. The interference contrast in Fig. 3c highlights the individual ribbons within a pixel.

with 9 intermediate supports. In the active area, where the channels and intermediate supports are located, there is no visible horizontal pixel boundary between two adjacent pixels. The boundary is defined by the electrical connection to ribbons made outside the active area (not shown). Figure 3b also illustrates line illumination of the linear array. The vertical and horizontal dimensions of the light output from a pixel are determined by the area of illumination and the horizontal pixel boundary.

MODEL FOR DEVICE OPERATION

A simple one-dimensional model for the conformal GEMS device provides insight into many key features of the static device operation. The electromechanical portion of the model assumes a distributed electrostatic force along the ribbon length, with negligible fringing fields at the ribbon edges. It also assumes that the tensile force due to stress dominates the bending force due to Young's modulus. Under these conditions, simple analytical expressions can be obtained to describe the ribbon profile as a function of voltage. It is beyond the scope of this paper to provide a detailed derivation of the model.

Ribbon displacement as a function of voltage contains well-known hysteresis that is characterized by two critical voltages: a pull-down voltage V_{PD} and a release voltage V_{RL}. Within the accuracy of our model, the two critical voltages are given by the expressions [6]

$$V_{PD} = \frac{1.673}{L} \sqrt{\frac{St^3}{\varepsilon_o}} \qquad (1)$$

$$V_{RL} = \frac{2}{L} \sqrt{\frac{S}{\varepsilon_o}} \left[\sqrt{(t-h)th} + (t-h)^{3/2} \ln\left(\frac{\sqrt{t} + \sqrt{h}}{\sqrt{t-h}}\right) \right], \qquad (2)$$

where $L = \Lambda - b_s$ is the ribbon length, b_s is the intermediate support width, h is the air gap, ε_o is the permittivity of free space,

$$S = \sum_p \sigma_p t_p \quad \text{and} \quad t = h + \sum_q \frac{t_q}{\varepsilon_q} .$$

Here, S is the tensile force per unit ribbon width, which depends on the stress σ_p and thickness t_p of each layer in the ribbons. t is the effective electrostatic thickness of the layers between the ribbon metal and the silicon substrate, with the thickness t_q of each dielectric layer reduced by its relative permittivity ε_q.

For $|V| < V_{RL}$, the ribbons are partially actuated and suspended above the substrate. For $|V| > V_{PD}$, the ribbons are fully actuated into contact with the standoffs and the length of ribbon in contact may be expressed as

$$b_c = L\left(1 - V_{RL}/V\right). \qquad (3)$$

The ribbons are bistable between these two voltages, $V_{RL} < |V| < V_{PD}$, with the bistable state depending on the most recent state.

Equation (3) can be used to couple the electro-mechanical portion of the model with an optical portion derived from scalar diffraction theory. The intermediate support width b_s is chosen to be equal to length b_c of ribbon in contact, i.e., $b_s = b_c = b$. In addition, the ribbon profile is approximated to be a trapezoid with linear sidewalls when the device is fully actuated. There is some curvature to the sidewalls in reality, as is evident from Figs. 2b and 2c. For an incident beam with wavelength λ, the diffraction efficiency η_m of the mth-order diffracted beam is given by the expression

$$\eta_m = \frac{64h^2}{m^2\pi^2\lambda^2} \left[\frac{m\left(1-\frac{2b}{\Lambda}\right)\cos\left(m\pi\frac{b}{\Lambda}\right)\sin\left(\frac{2\pi h}{\lambda}-\frac{m\pi}{2}\right)}{m^2(1-2b/\Lambda)^2 - 16h^2/\lambda^2} \right.$$
$$\left. + \frac{\frac{4h}{\lambda}\sin\left(m\pi\frac{b}{\Lambda}\right)\cos\left(\frac{2\pi h}{\lambda}-\frac{m\pi}{2}\right)}{m^2(1-2b/\Lambda)^2 - 16h^2/\lambda^2} \right]^2 .$$

$$(4)$$

More generally, the efficiency from an arbitrary ribbon profile $y(x)$ can be determined from the integral [7]

$$\eta_m = \left| \frac{1}{\Lambda} \int_0^{\Lambda} e^{i4\pi y(x)/\lambda}\, e^{-i2\pi mx/\Lambda}\, dx \right|^2 . \qquad (5)$$

For a trapezoidal profile with $b_s \neq b_c$, the integral can still be evaluated in closed form, but yields a rather lengthy expression. Equations (4) and (5) neglect the gaps between ribbons and assume perfect reflectivity for the ribbon metal.

It is instructive to compare the expected optical efficiency of an ideal conformal GEMS device with an ideal GLV. For the square grating profile of a GLV, Eq. (4) is evaluated with $b = 0.5\,\Lambda$, whereas for a typical conformal GEMS device $b \sim 0.3\,\Lambda$. Table 1 summarizes the results for gratings that maximize first-order efficiency and those intended for multi-order systems that minimize reflected light (0th order). In a system that collects one or both first orders, the device efficiency is slightly greater for a GLV than for a conformal GEMS. In a multi-order system, the conformal GEMS device is usually more efficient. It should be noted that the optimal depth of the square grating profile is $h = 0.25\,\lambda$ independent of which orders are collected. The optimal depth of the trapezoidal profile is dependent on the orders collected.

Table 1 Comparison of Diffraction Efficiencies

Grating Profile	Optimal Depth for Specified Order		Order Efficiency (%)				
			0	±1	±2	±3	±4
Trapezoid $b/\Lambda = 0.3$	min 0	$h/\lambda = 0.304$	0	34.9	8.10	2.89	3.08
	max ±1	$h/\lambda = 0.258$	4.63	37.7	5.25	2.33	1.93
Square $b/\Lambda = 0.5$	min 0	$h/\lambda = 0.25$	0	40.5	0	4.50	0
	max ±1	$h/\lambda = 0.25$	0	40.5	0	4.50	0

We have developed a more general numerical model that couples diffraction theory with an electromechanical model for the actual nontrapezoidal profile of the ribbon surface. However, the simple model described above is sufficiently accurate to understand the basic device principles.

DEVICE PERFORMANCE

Figure 4 shows the measured response of a fabricated conformal GEMS device as a function of ribbon voltage. These results were obtained by illuminating the device with a 680 nm laser beam and measuring the light output in the 0th and 1st orders, while driving the device with a bipolar 10 KHz triangle wave. At this relatively low frequency, the device response is essentially instantaneous and is the same as the static response to a DC voltage. Bipolar actuation waveforms prevent charge accumulation in the dielectric layers [8]. The plot in Fig. 4 shows only the response to positive voltages. The negative voltage response is identical, because the electrostatic force is proportional to the square of the applied voltage. The curves for the 0th and 1st orders contain the anticipated hysteresis. Below the release
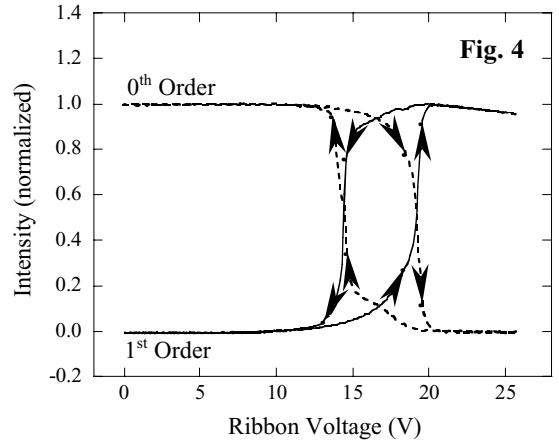
Fig. 4 Measured light intensity in the 0th and 1st order beams as a function of applied voltage showing hysteresis. The arrows in the bistable region indicate the permitted direction of travel.

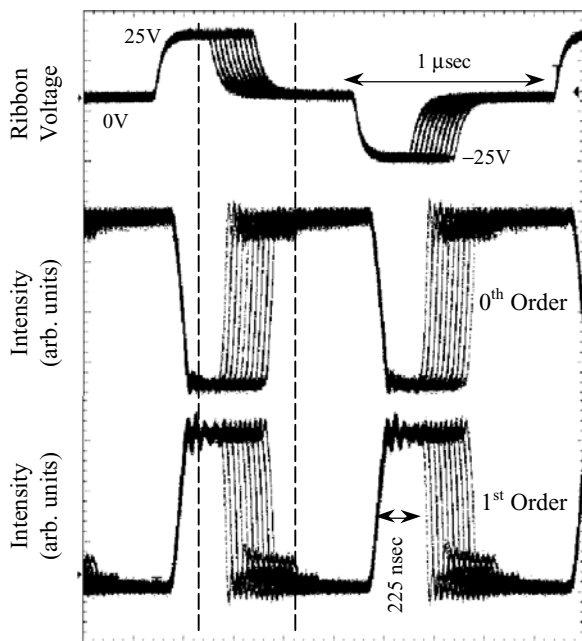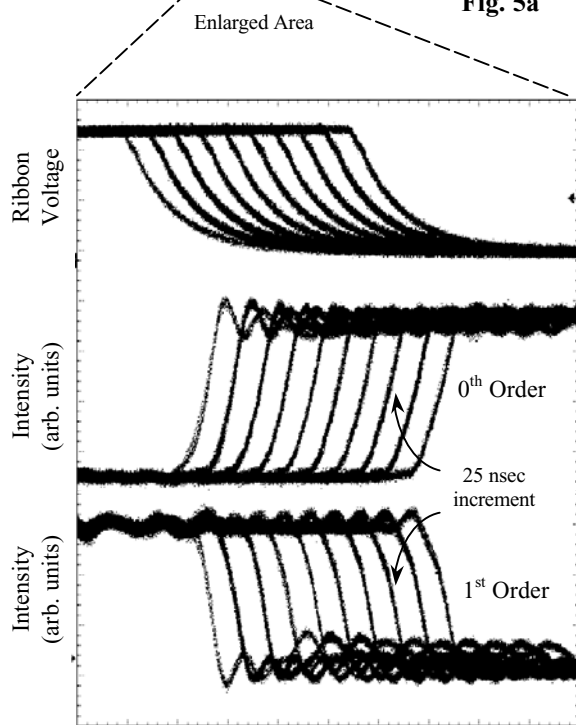**Fig. 5a**

Enlarged Area

Fig. 5b

Fig. 5 Oscilloscope traces of the high-speed response of a conformal GEMS device to a random PWM data stream, showing the 0th and 1st order light intensities.
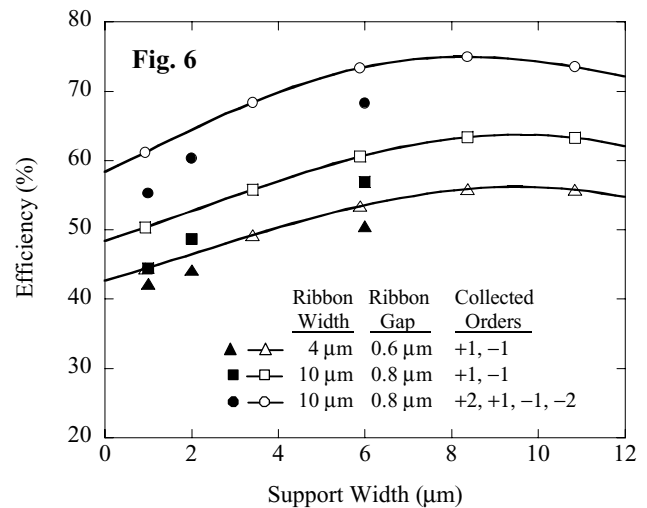

Fig. 6 Plot of device diffraction efficiency for various device designs comparing experimental results (filled markers) with theory (solid lines with open markers).

voltage, the ribbons are suspended (partially actuated) above the substrate and only a small percentage of the incident light is diffracted out of the 0th order. Above the pull-down voltage, the ribbons are fully actuated and nearly all of the incident light is diffracted out of the 0th order into the nonzero diffracted orders. In between these two critical voltages, the response is bistable and depends on the most recent state.

For this particular device, ribbon length L is 35 μm, gap h is 180 nm, effective electrostatic thickness t is 231 nm, and the tensile force per unit width S is 117 nt/m. These values for S and t are computed based on the known thickness of the device layers and estimated stress and permittivity. Equations (1) and (2) predict a pull-down voltage of 19.3 V and a release voltage of 13.0 V. These theoretical critical voltages are in agreement with the experimental hysteresis curves in Fig. 4.

The device is intended to be used digitally by switching the applied voltage between 0 V and $\pm V_{ON}$, where V_{ON} is enough above the pull-down voltage to ensure stable device operation. Figure 5 shows the dynamic response of the above device to a digital pulse-width modulated (PWM) data stream. The applied voltage is a random bipolar waveform with 10 different pulse-length separated by 25 nsec intervals. The optical rise times are ~30 nsec during turn-on and ~50 nsec during turn-off with edge jitter less than 0.5 nsec (see Fig. 5b).

The response to the random PWM data stream illustrates the device use in an imaging application. For example, the integrated 1st order intensity could be used to define multiple gray levels in an image. The low jitter enables formation of fine gray levels. The particular driver rise times and device geometry in this experiment were chosen to keep ringing in the optical response relatively small. More ringing can be tolerated in imaging systems, because only the integrated intensity is important in generating a digital gray scale.

Finally, the device design can be optimized for diffraction efficiency by adjusting the dimensions of structural features. Figure 6 shows the multi-order diffraction efficiency as a function of intermediate support width b_s for devices with a 31 μm period illuminated with a 670 nm semiconductor laser. The measured efficiencies are scaled to compensate for imperfect reflectivity of the ribbon metal and loss caused by reflections from the optical window used in the device packaging. As expected, the efficiency depends strongly on the specific diffracted orders used by the optical system and on the duty cycle of the semiconformal grating, which is determined primarily by the intermediate support width.

The theoretical curves in Fig. 6 are computed using the simple trapezoidal model with $b_s \neq b_c$ discussed earlier. To determine the portion of each ribbon in contact with the substrate, i.e., to determine b_c, the operating voltage is taken to be 110% of the pull-down voltage. In addition, the calculated efficiencies are reduced to appropriately take into account the gaps between ribbons. The trapezoidal model tends to overestimate the measured diffraction efficiency by a few percent. Ribbon curvature, ignored by the model, effectively increases the contact portion of the ribbons. For the devices considered in Fig. 6, this increase in b_c would decrease efficiency.

CONCLUSION

We have developed a unique spatial light modulator, the conformal GEMS device, which contains a linear array of optical MEMS gratings and provides high-speed digital light modulation. The optical performance, speed, and potential low cost of the device make it attractive for digital light modulation systems such as printers and displays. Our prototype devices are 256-pixel linear arrays with a contrast greater than 2000:1. An initial reliability study shows that the device should be capable of meeting the requirements of the most demanding systems. Ongoing investigations include improvement of device design, incorporation of devices into application systems and development of linear arrays with greater pixel count.

REFERENCES

[1] N. K. Sheridon, "The Ruticon Family of Erasable Image Recording Devices", IEEE Trans. Electron Devices **ED-19**, 1003-1010 (1972).

[2] W. Brinker, W. Wirges, G. Przyrembel, R. Gerhard-Multhaupt, J. Klemberg-Sapieha, L. Martinu, D. Poitras, and M. R. Wertheimer, "Metallized Viscoelastic Control Layers for Light-Valve Projection Displays", Displays **16**, 13-20 (1995).

[3] O. Solgaard, F. S. A. Sandejas, and D. M. Bloom, "Deformable Grating Optical Modulator", Opt. Lett. **17**, 688-690 (1992).

[4] D. T. Amm and R. W. Corrigan, "Optical Performace of the Grating Light Valve Technology", SPIE Proc. **3634**, 71-77 (1999).

[5] M. W. Kowarz, "Spatial Light Modulator with Conformal Grating Device", U. S. Patent 6,307,663, Oct. 23, 2001.

[6] Equation (1) for V_{PD} agrees with the empirical fit result from P. M. Osterberg and S. D. Senturia, "M-Test: A Test Chip for MEMS Material Property Measurement Using Electrostatically Actuated Test Structures", IEEE J. Microelectromech. Syst. **6**, 107-118 (1997), Table III.

[7] See, for example, M. Bass (ed.), *Handbook of Optics* (McGraw-Hill, New York, 1995), Vol. II, Section 8.4.

[8] M. W. Kowarz, D. Karns, B. E. Kruschwitz and J. C. Brazas, Jr., "Method and System for Actuating Electro-Mechanical Ribbon Elements in Accordance to a Data Stream", U. S. Patent 6,144,481, Nov. 7, 2000.